This project has received funding from the European Union's Horizon 2020 research and innovation programme under grant agreement No 727616.

Biofficiency

Material investigations for FB combustion systems

(D3.1)

Authors: Patrik Yrjas, Li Na
Version: Final
Quality Review: Person 2
Date: 26.02.2018
Partners involved: Abo, Valmet

Grant Agreement No. 727616
Starting Date: 01.11.2016
Duration: 36 months

Disclaimer

The content of this deliverable does not reflect the official opinion of the European Commission. Responsibility for the information and views expressed herein lies entirely with the author(s).

Table of Contents

1. Description of task

1.1. Objective

One of the main objective of this project is to investigate the possibilities to increase the steam temperature in biomass fired boilers to around 600 °C from today´s values around 500-550 °C. The limiting factor for increasing the steam temperature is superheater high-temperature corrosion, which most often is caused by alkali chlorides originating from the fuel(s).

There are several different ways of reducing the risk for corrosion caused by alkali chlorides, e.g. the use of additives (e.g. kaolinite, ammonium sulphate, iron sulphate) or intelligent co-combustion with fuels containing alumina silicates and/or sulphur or pre-treatment of fuels (e.g. torrefaction, washing, heat explosion). Another alternative to avoid corrosion is to choose the right superheater material. Accordingly, the purpose of this task was to determine the corrosion sensitivities of certain superheater materials chosen by the industrial partners under conditions typical for fluidised bed boilers burning different types of biomass fuels such as e.g. bark and wheat straw.

2. Methodology

2.1. Experimental method and evaluation

Four boiler materials were chosen together with Valmet Technologies for the tests. Valmet also delivered the materials, which are listed in Table 1.

Table 1. The composition of steels (wt-%)

	C	***Mn***	***P***	***S***	***Si***	***Cr***	***Ni***	***Mo***	***N***	***Nb***	***Cu***	***Al***	***B***
304H	0.04-0.1	2.0	0.045	0.030	1.0	18-20	8-11	-	-	-			-
304HCu	0.07-0.13	1.0	0.040	0.010	0.3	17-19	7.5-10.5	-	0.05-0.12	-	2.5-3.5	0.003-0.03	0.001-0.01
310HCbN	0.04-0.1	2.0	0.045	0.030	1.0	24-26	19-22	-	0.15-0.35	0.20-0.60			-
347HFG	0.06-0.1	2.0	0.045	0.030	1.0	17-19	9-13	8xC-1.10	-	-			-

The materials were cut to coupons with a size of approximately 20 x 20 x 5 mm. The top surfaces were subsequently polished by a 320 and a 1000 grid silicon carbide grinding paper to get a smooth surface. Then the specimens were cleaned in ethanol in ultrasound bath and further pre-oxidised in 200 °C for 24 h. A pre-determined salt mixture, simulating a simplified deposit, was then placed on each coupon before exposure (0.25 g/specimen). Five different salt mixtures were used in the tests. These were also determined in cooperation with Valmet. The chemical compositions and the first melting points (T_0) of the five salts are shown in Table 2.

The exposures were carried out in a horizontal tube furnace for 168 h at 600 and 650 °C. One setup (Figure 1a) was made of a standard horizontal tube furnace in which the samples were exposed to ambient air while another setup included a pre-heater, water pump, and gas lines. The water was heated up to 200 °C and then introduced into the furnace together with the chosen gas mixture (Figure 1b). The gas atmosphere used in the tests composed of 6 % O_2, 80 ppm SO_2, 15 % H_2O and balanced with N_2.

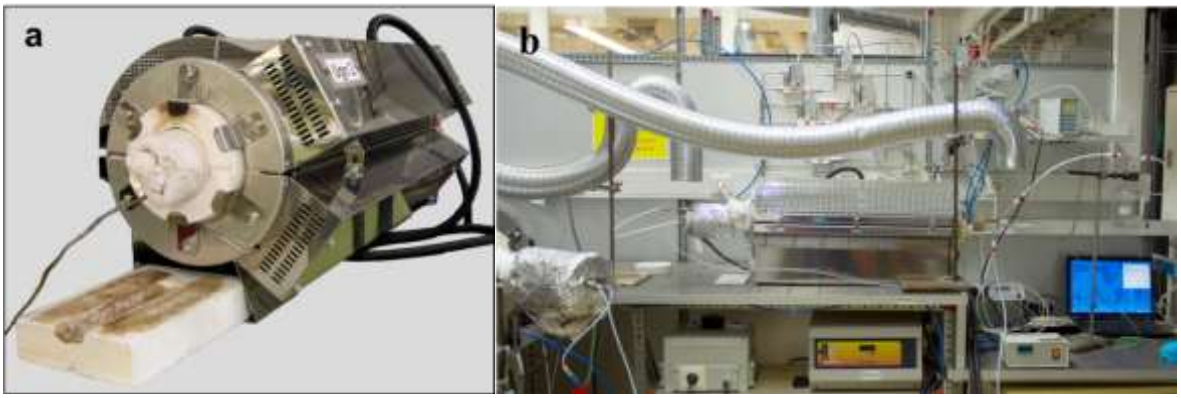

Figure 1. Horizontal tube furnaces for corrosion tests a) ambient air and b) gas mixture + H_2O (pictured by Linus Silvander).

Table 2. The compositions and the first melting points (T_0) of the synthetic ashes.

#	*Salts*	*Compositions (wt%)*	*T_0 (°C)*
1	KCl	100	771
2	$5KCl+95K_2SO_4$	5/95	690
3	$5KCl+95CaSO_4$	5/95	681
4	$15KCl+85K_2SO_4$	15/85	690
5	$15KCl+85CaSO_4$	15/85	681

After 168 h, the furnace and the H_2O and SO_2 flows were turned off, while the pre-heater was turned off 30 minutes later. The specimens were allowed to cool down inside the furnace in a

continuous flow of an O_2-N_2 mixture until room temperature was reached. The samples were then taken out from the tube, placed in a mould and cast in epoxy, then cut off in the middle to reveal the specimen's cross-section. The cross-section surfaces were further polished by 320, 1000 and 1200 grid SiC papers using kerosene as lubricant. After polishing, the specimens were cleaned in petroleum ether in an ultrasound bath and sputtered with carbon. The specimens were then studied and analysed by means of a scanning electron microscope equipped with energy dispersive x-ray analyser (SEM/EDXA). The corrosion layer thickness was determined by combining several back-scatter images into one panoramic image. After that, each panoramic image was digitally treated by using contrast differences. An example of the treatment stages of a typical SEM panoramic image is shown in Figure 2. Often but not always the oxide layer is detached from the steel surface and this is believed to occur during cooling maybe due to different expansion degrees of the oxide layer compared to the steel material. The reason is not due to sawing or polishing, since then the oxide layer would be expected to be more broken and uneven. After the panoramic images were colored, the thickness of the oxide layers were determined for each vertical line of pixels and recalculated into µm. The corrosion layers are then defined as the thickness of the oxide layer for each line and the corrosion attack is expressed as the mean thickness of the oxide layer. In each case, an area chosen from the corrosion layer was analysed in the SEM backscatter electron mode to identify the distribution and relative amounts of the elements.

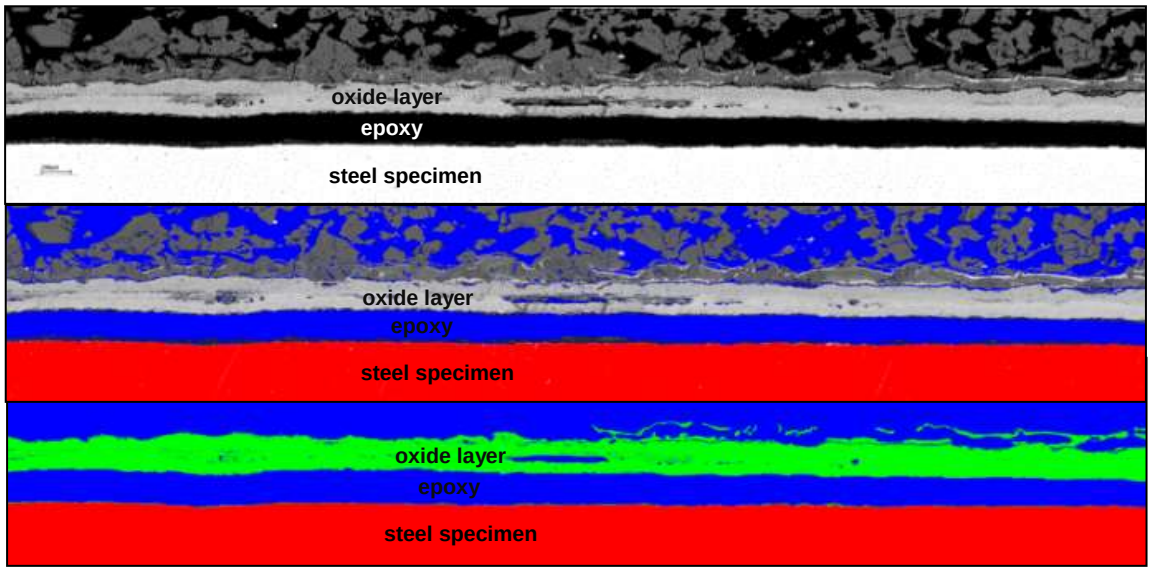

Figure 2. A schematic view of the colouring stages of a SEM panoramic image in order to determine oxide layer thickness.

The method described above have been used and published in several previous projects and doctoral thesis works where more details and discussions of the method can be found [1-5].

3. Results and discussion

The full test matrix from the tests performed is presented in Table 3 and a summary of all the oxide layer thickness results are presented in Table 4.

Table 3. The test matrix.

Temperature	*Salt*	*Gas atm*	*Material*
650 °C	5KCl-95K_2SO_4	ambient air	304H
650 °C	5KCl-95K_2SO_4	ambient air	304HCu
650 °C	5KCl-95K_2SO_4	ambient air	310HCbN
650 °C	5KCl-95K_2SO_4	ambient air	347HFG
650 °C	5KCl-95$CaSO_4$	ambient air	347HFG
650 °C	5KCl-95K_2SO_4	5%O_2-80 ppm SO_2-15% H_2O-rest N_2	304H
650 °C	5KCl-95K_2SO_4	5%O_2-80 ppm SO_2-15% H_2O-rest N_2	304HCu
650 °C	5KCl-95K_2SO_4	5%O_2-80 ppm SO_2-15% H_2O-rest N_2	310HCbN
650 °C	5KCl-95K_2SO_4	5%O_2-80 ppm SO_2-15% H_2O-rest N_2	347HFG
650 °C	5KCl-95$CaSO_4$	5%O_2-80 ppm SO_2-15% H_2O-rest N_2	347HFG
600 °C	5KCl-95K_2SO_4	5%O_2-80 ppm SO_2-15% H_2O-rest N_2	304H
600 °C	5KCl-95K_2SO_4	5%O_2-80 ppm SO_2-15% H_2O-rest N_2	304HCu
600 °C	5KCl-95K_2SO_4	5%O_2-80 ppm SO_2-15% H_2O-rest N_2	310HCbN
600 °C	5KCl-95K_2SO_4	5%O_2-80 ppm SO_2-15% H_2O-rest N_2	347HFG
600 °C	KCl	5%O_2-80 ppm SO_2-15% H_2O-rest N_2	347HFG
600 °C	15KCl-85K_2SO_4	5%O_2-80 ppm SO_2-15% H_2O-rest N_2	304H
600 °C	15KCl-85K_2SO_4	5%O_2-80 ppm SO_2-15% H_2O-rest N_2	304HCu
600 °C	15KCl-85K_2SO_4	5%O_2-80 ppm SO_2-15% H_2O-rest N_2	310HCbN
600 °C	15KCl-85K_2SO_4	5%O_2-80 ppm SO_2-15% H_2O-rest N_2	347HFG
600 °C	15KCl-85$CaSO_4$	5%O_2-80 ppm SO_2-15% H_2O-rest N_2	347HFG

Table 4. Summary of the results.

Temp. [°C]	*Atmosphere*	*Salt*	*Steel*	*Mean [µm]*	*Median [µm]*	*Most recurring [µm]*	*Max. [µm]*	*Min. [µm]*
650 °C	Air	2	304H	39.3	39.5	42.2	76.9	4.3
650 °C	Air	2	304HCu	83.6	83.6	62.1	187.9	0.0
650 °C	Air	2	310HCbN	17.3	8.2	5.1	106.6	0.0
650 °C	Air	2	347HFG	29.0	27.3	7.0	84.8	0.0
650 °C	Air	3	347HFG	32.6	32.4	1.2	91.0	0.0
650 °C	Gas	2	304H	73.2	70.3	64.1	131.2	16.0
650 °C	Gas	2	304HCu	73.5	71.9	57.8	71.9	73.5
650 °C	Gas	2	310HCbN	24.1	16.8	1.2	120.7	0.0
650 °C	Gas	2	347HFG	46.1	37.9	20.3	165.2	0.4
650 °C	Gas	3	347HFG	26.5	23.8	11.3	65.6	3.1
600 °C	Gas	2	304H	23,5	18,4	10,2	87,5	0,4
600 °C	Gas	2	304HCu	18.5	17.6	14.8	37.5	1.6
600 °C	Gas	2	310HCbN	7.3	7.0	6.6	14.5	0.0
600 °C	Gas	2	347HFG	19.3	18.0	11.7	43.0	3.5
600 °C	Gas	1	347HFG	4.6	4.7	4.7	9.4	0.0
600 °C	Gas	4	304H	8.8	8.2	8.2	21.9	0.8
600 °C	Gas	4	304HCu	4.7	4.7	4.3	14.8	0.0
600 °C	Gas	4	310HCbN	3.0	3.1	3.1	8.6	0.0
600 °C	Gas	4	347HFG	5.1	5.1	5.1	23.8	0.0
600 °C	Gas	5	347HFG	5.3	5.1	5.1	14.5	0.4

Figure 3 shows a summary of the results from the tests with the KCl-K_2SO_4 salts. 310HCbN containing higher amount of Ni and Cr showed great corrosion resistant. The oxide layer formed was detectable but quite low at 600 °C. When exposed to 650 °C in air, the scale of corrosion layer was ~17 µm, which is still recognized as medium to low corrosion. Significant corrosion was identified when the thickness of the oxide layer increased to 24 µm in simulated flue gas atmosphere (Figure 3 and Figure 4a).

At 650 °C, 304HCu and 304H suffered from high corrosion in flue gas atmosphere. The thicknesses of the oxide layers were over 70 µm, while the thickness of the oxide layer for 347HFG was determined to be 46 µm, which also is significant. Figures 4b and 4c show typical corrosion layers represented by 304HCu and 304H. Both the outer oxide layer and the internal oxidation of the materials are clearly observed. The salt mixture/oxide layer seems to have been

partly molten and the corrosion products have diffused and formed a covering layer on the salt particles. At 650 °C, the oxide layer thicknesses were generally somewhat lower in air than in the cases with simulated flue gas. Nevertheless, the oxide layers were also in these cases high. At 600 °C, most steels managed fairly well in the tests with KCl-K_2SO_4.

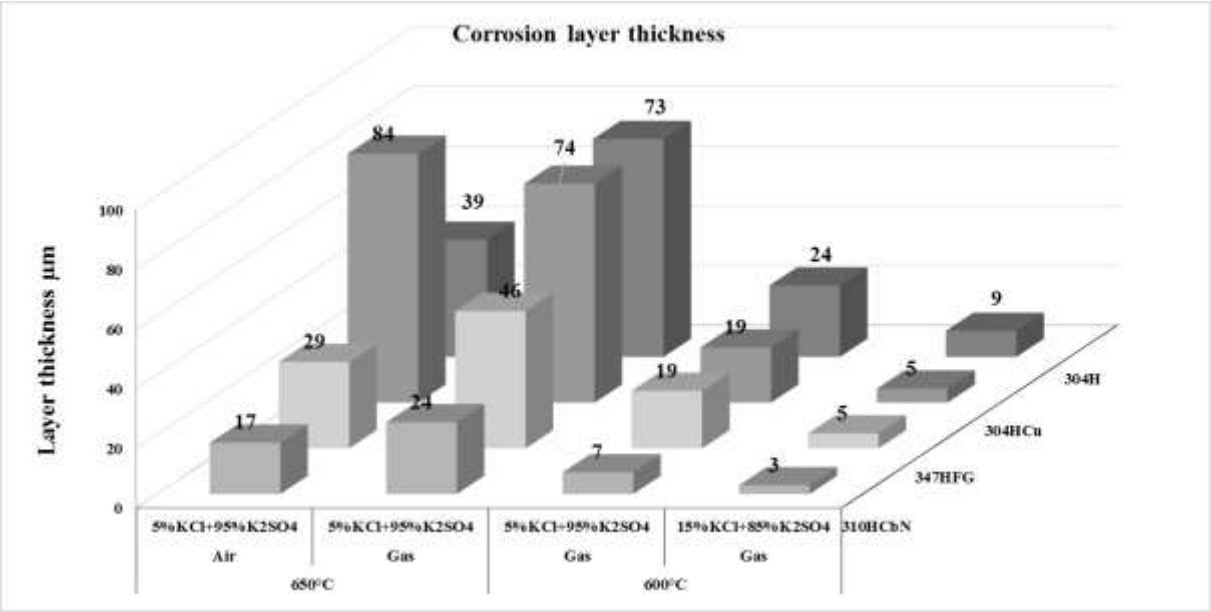

Figure 3. Results from the tests performed at 650°C in air and in simulated flue gas with 5%KCl+95%$K_2SO_4$and at 600°C in flue gas with 5%KCl+95%K_2SO_4 and 15%KCl+85%K_2SO_4.

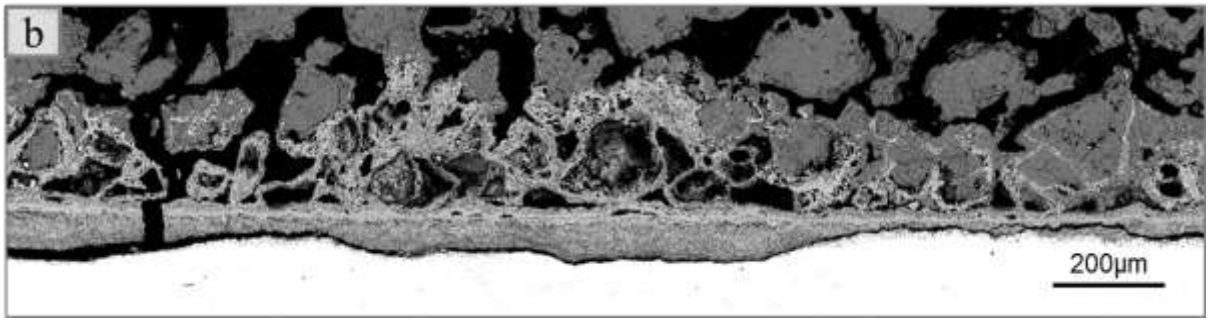

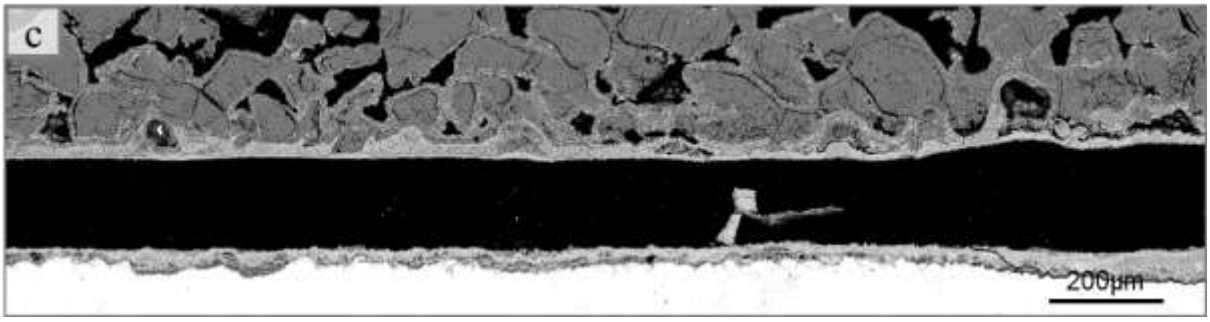

Figure 4. The panorama images of a) 310HCbN, b) 304HCu and c) 304H after exposure to simulated flue gas with 5KCl-95K_2SO_4 at 650 °C.

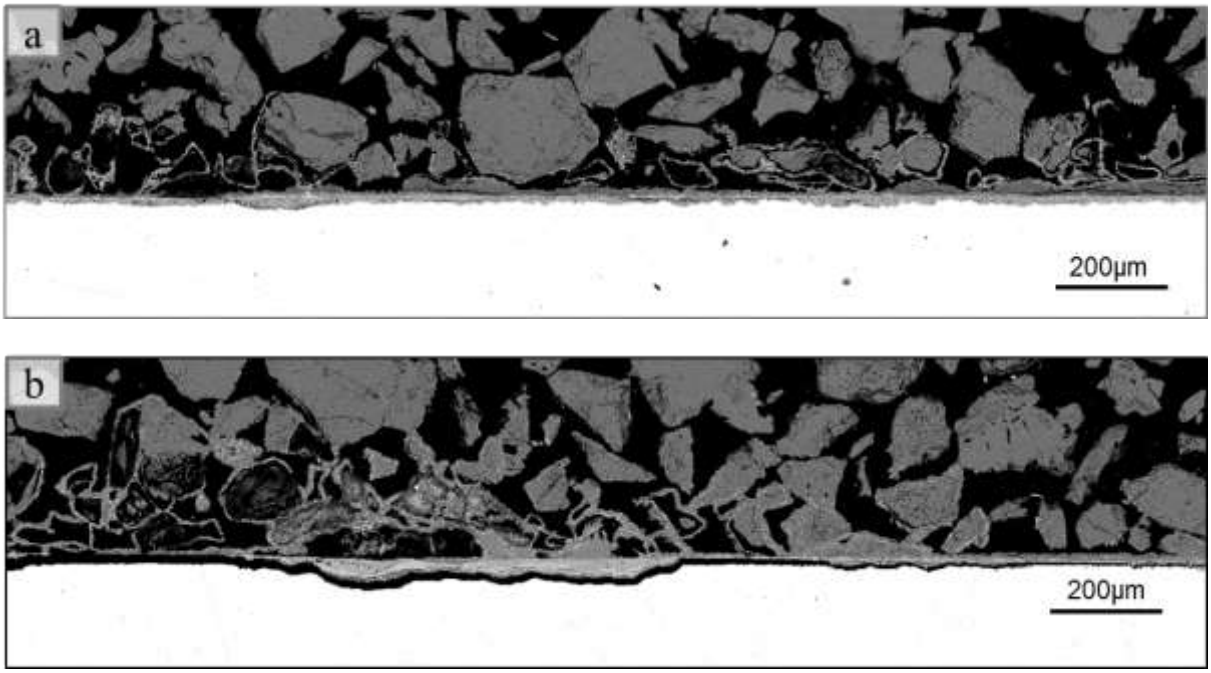

Figure 5. The panorama images of a) 304HCu and b) 304H after exposure to simulated flue gas with 5KCl-95K_2SO_4 at 600 °C.

Figure 6 shows an example of an elemental map representing 304HCu after being exposed to flue gas at 650 °C. It can be observed that Fe was depleted from the entire internal corrosion layer and Cr is left. No remaining Cl was detected. It can also be seen that S is found in the oxide layer together with Cr while Ni is depleted. For the other steels, the x-ray mapping of the elements found in the oxide layer gave similar information except that some Fe was detected in the internal oxide layer too.

Figure 7 shows the same as Figure 6 except that the exposure was in air. It can be seen that Fe is depleted and has formed an iron oxide layer around the salt particles, together with some Cu. In addition, it can be noted that no sulphur is part of the oxide layer as was in the case with flue gas where sulphur was in the gas mixture.

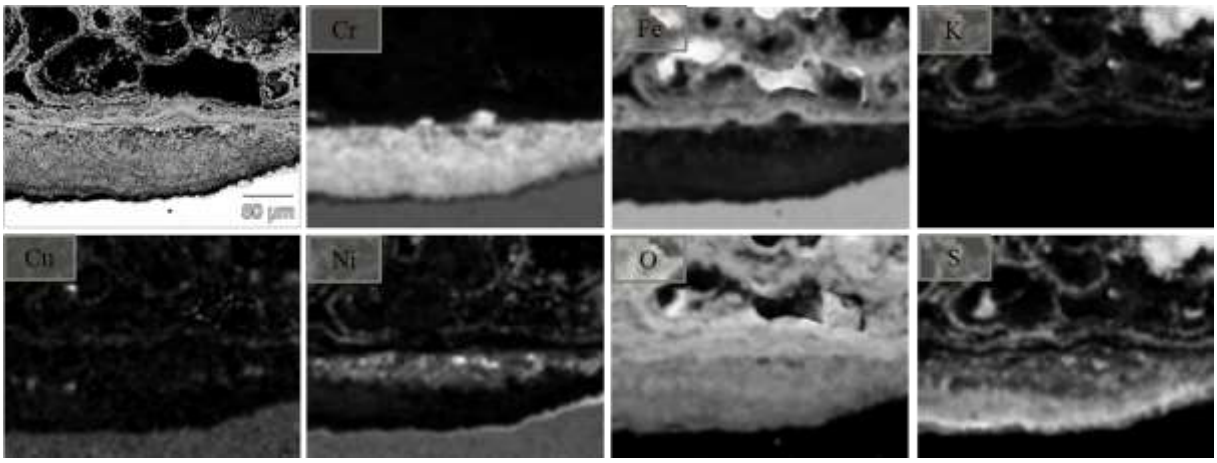

Figure 6. The X-Ray Maps of 304HCu after exposure to simulated flue gas with 5KCl-95K_2SO_4 at 650 °C.

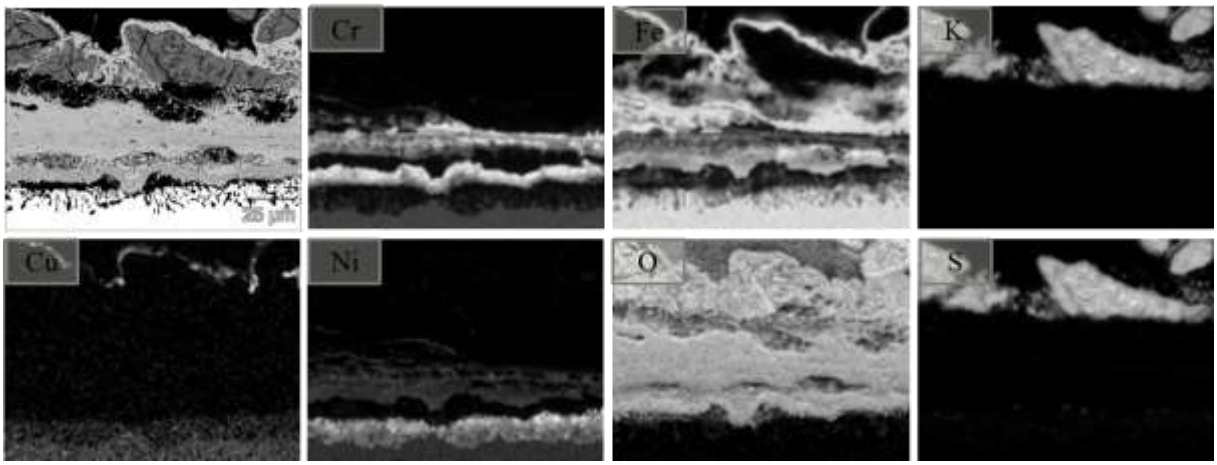

Figure 7. The X-Ray Maps of 304HCu after exposure to air with 5KCl-95K_2SO_4 at 650 °C.

Figure 8 illustrates the oxide layer thicknesses of 347HFG after being exposed to salts containing different amounts of Cl. It can be observed that there is a strange decrease of the layer thickness with increasing amount of Cl when exposed to the flue gas at 600 °C. Figure 9 shows the morphology of the oxide layers formed. With pure KCl, a homogenous and compact K_2SO_4 layer was identified to attach on the thin oxide layer as shown in Figure 10. In addition, the salt above the steel surface was analysed after exposure and obviously, K_2SO_4 was rapidly formed on the surfaces of the KCl particles (Figure 11). The formation of K_2SO_4 may have suppressed the corrosivity of KCl and protected the steel. However, this sulphating effect does not explain why the corrosion is lower with 15 % KCl than with 5 % KCl, and the reason remains unclear for now.

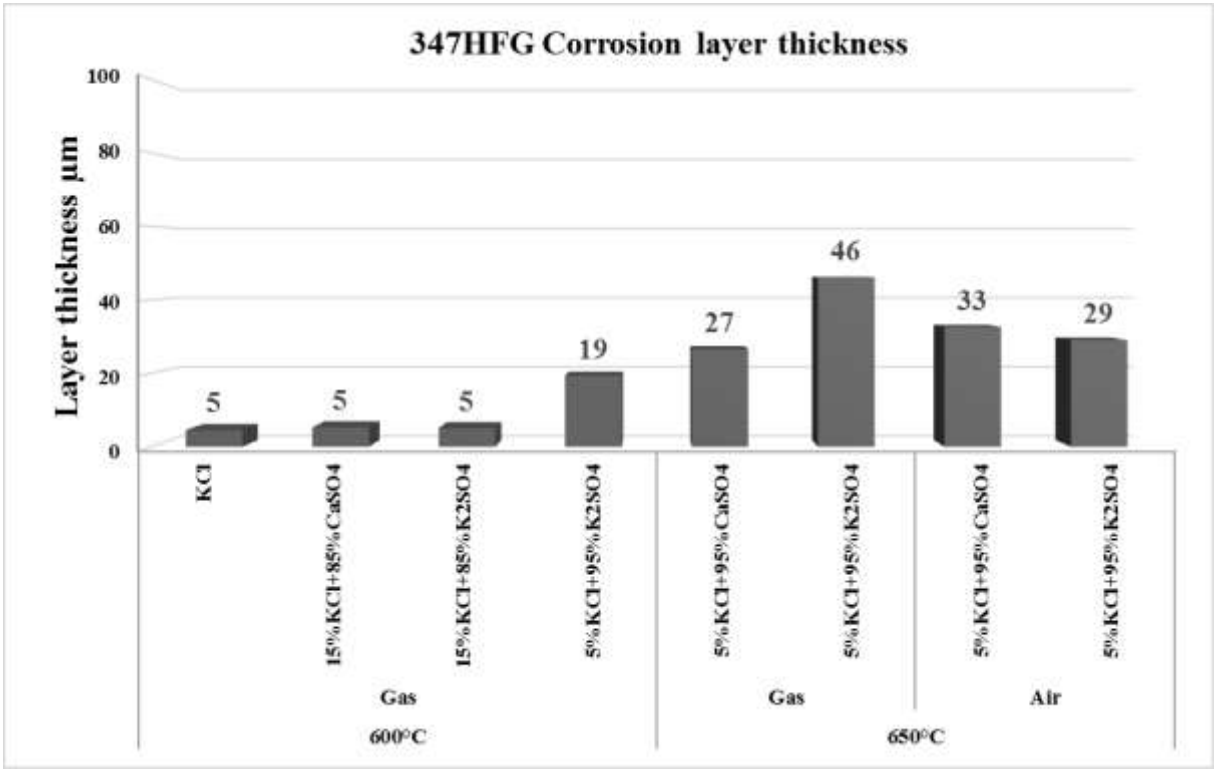

Figure 8. The mean oxide layer thicknesses of 347HFG after exposure to 600 °C and 650 °C in flue gas atmosphere and in air with different salt mixtures.

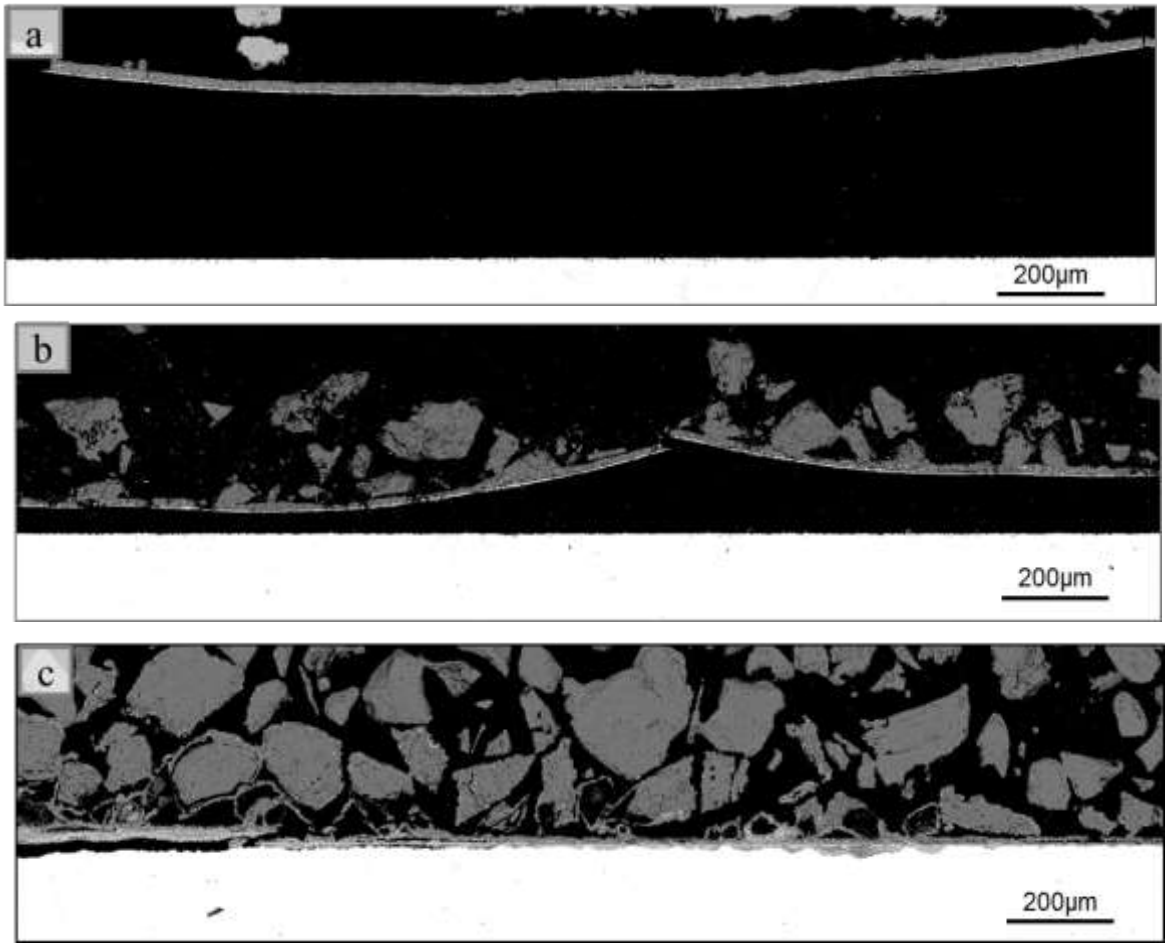

Figure 9. Panorama images of 347HFG after exposure to 600 °C in flue gas with a) KCl, b) 15KCl-85K_2SO_4 and c) 5KCl-95K_2SO_4.

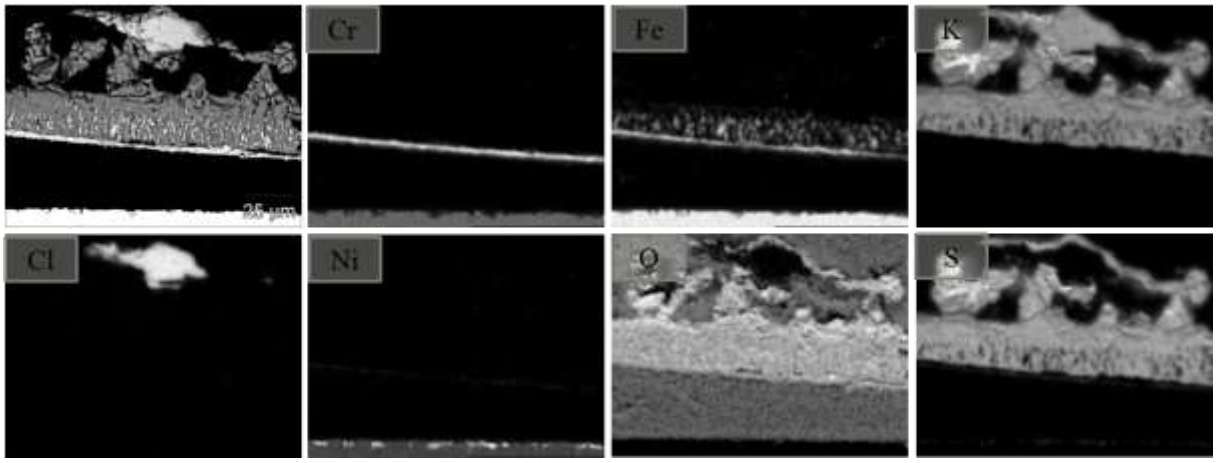

Figure 10. X-Ray Maps of 347HFG after exposure to simulated flue gas with KCl at 600 °C.

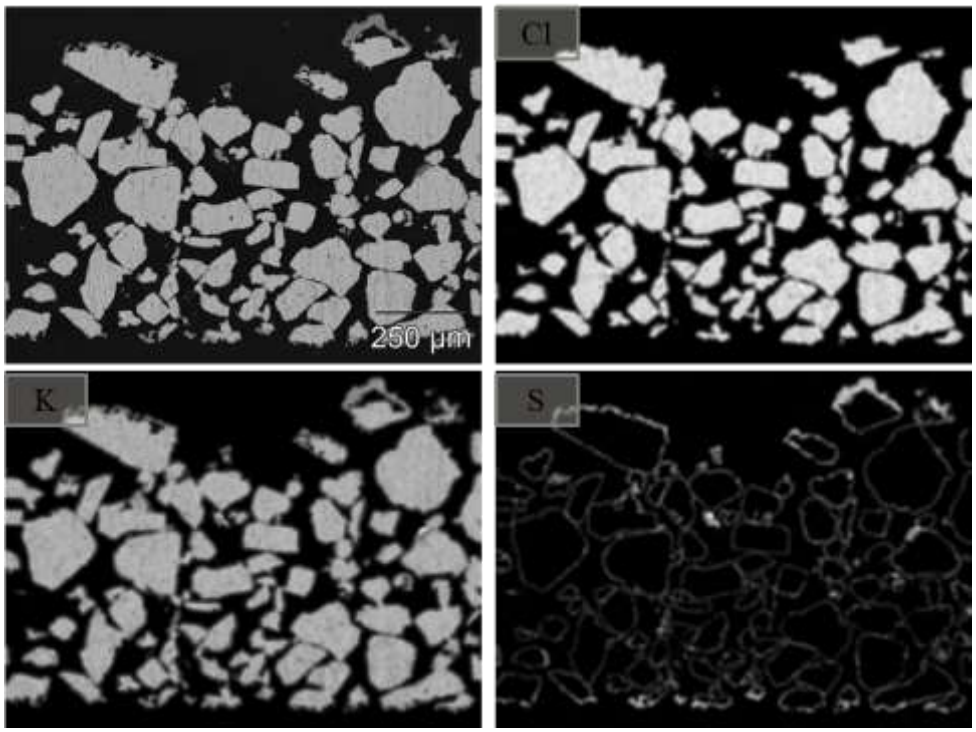

Figure 11. X-Ray Maps of salt particles above the oxide layer on the steel surface of 347HFG after exposure to simulated flue gas with KCl at 600 °C.

Figure 8 also compares the results from the tests with KCl-$CaSO_4$ and KCl-K_2SO_4. At 600 °C, no significant difference was observed on the oxide layer with these two salts. In addition, no significant differences was observed on the oxide layer after exposure to 650 °C in air with these two salts. After exposure to flue gas atmosphere at 650 °C, the morphology of the corrosion layers appears to be somewhat different (Figures 12a and 12b). For 5KCl-95K_2SO_4, the corrosion layer could be distinguished as two parts, outer oxide layer and internal oxide layer. The detailed compositions of the layers were similar as that shown in Figure 6, except for the Cu. For 5KCl-95$CaSO_4$, other than the outer oxide layer, the steel also suffered severe grain boundary corrosion (Figure 13). The grain boundary corrosion could even reach as deep

as 30 µm. The loose grains were strongly depleted from Fe, while the inner grains were depleted from both Fe and Cr.

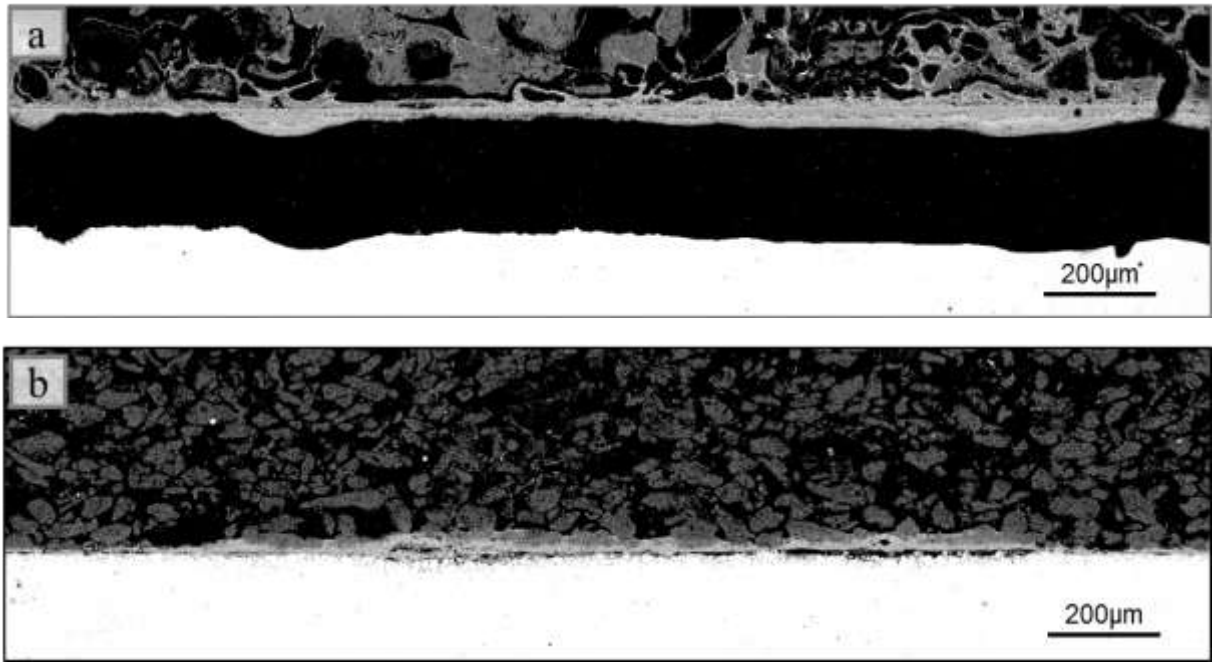

Figure 12. Panorama images of 347HFG after exposure to simulated flue gas at 650 °C with a) 5KCl-95K_2SO_4 and b) 5KCl-95$CaSO_4$.

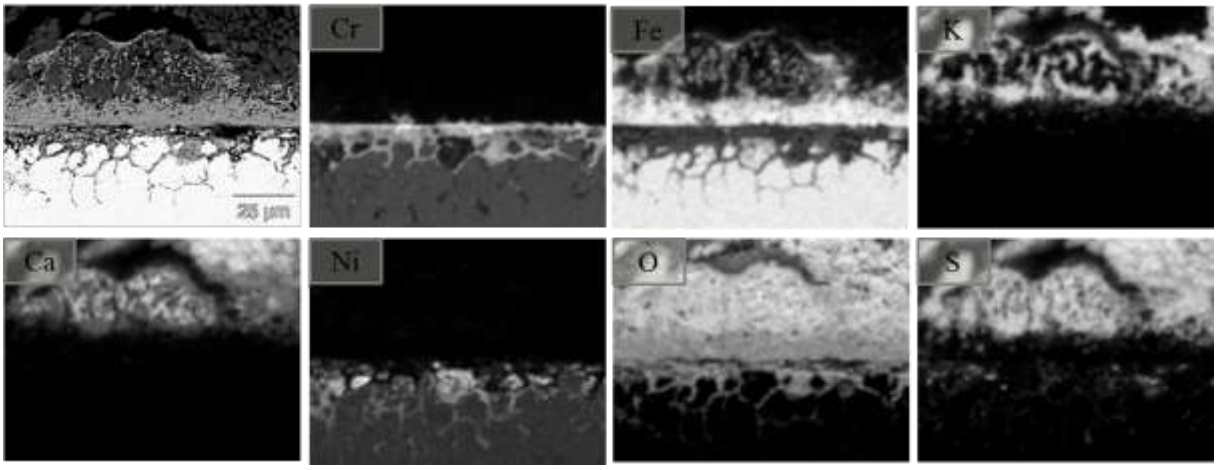

Figure 13. X-Ray Maps of 347HFG after exposure to simulated flue gas with 5KCl-95$CaSO_4$ at 650 °C.

4. Conclusions

High-temperature laboratory corrosion experiments have been done with four different steel qualities (304H, 304HCu, 310HCbN, and 347HFG). The steels were cut into coupons, then covered with salt mixtures containing different amounts of KCl, K_2SO_4 and $CaSO_4$, mimicking a chemically simplified deposit, and exposed to 600 or 650 °C in a tube furnace. The gas atmosphere consisted of either air or a synthetic flue gas (6 % O_2, 15 % H_2O, 80 ppm SO_2, and 79% N_2). The severeness of the corrosion is in this report given as the average value of the

measured oxide layer thickness, and as a rule of thumb if 20 µm is exceeded the corrosion can be regarded as risky.

Generally, it can be concluded that all materials managed relatively well at 600 °C, and only 304H corroded more than 20 µm (24 µm). However, both 304HCu and 347HFG formed oxide layers very close to 20 µm (both 19 µm) and therefore it is concluded that there is some risk of material loss. At 650 °C all materials exceeded 20 µm, and only 310HCbN was close to this limit (24 µm), while the others were clearly above.

Further, it could be observed that the presence of SO_2 in the gas decreased the corrosivity of KCl due to sulphation. However, higher corrosion was measured when the salt mixture contained 5% KCl compared to 15 and 100 %. The reason for this is unclear and would need more detail studies and analyses.

Finally, as previously mentioned, the main conclusion is that the materials behaved satisfactorily at 600 °C, but not at 650 °C. If the steels were to be ranked, based on this work, the order is as follows (best first): 310HCbN > 347HFG > 304HCu > 304H.

References

1. Skrifvars B.-J., Backman R., Hupa M., Salmenoja K., and Vakkilainen E., *"Corrosion of superheater steel materials under alkali salt deposits. Part 1: The effect of salt deposit composition and temperature*, Corrosion Science 50, 1274-1282, 2008.
2. Bankiewicz D., Yrjas P., and Hupa M., *"High-temperature corrosion of superheater tube materials exposed to zinc salts"*, Energy & Fuels 23, 3469-3474, 2009.
3. Bankiewicz D., *"Corrosion behaviour of boiler tube materials during combustion of fuels containing Zn and Pb",* Doctoiral thesis, Åbo Akademi University, ISBN 978-952-12-2746-2, 2012
4. Lehmusto J., *"The role of potassium in the corrosion of superheater materials in boilers firing biomass",* Doctoral thesis, Åbo Akademi University, ISBN 978-952-12-2960-2, 2013.
5. Hao Wu, *"Chemistry of potassium halides and their role in corrosion in biomass and waste firing",* Doctoral thesis, Åbo Akademi University, ISBN 978-952-12-3400-2, 2016.